

# Hessian Spectral Analysis at Foundation Model Scale

Diego Granziol<sup>1</sup> Khurshid Juarev<sup>2</sup>

## Abstract

Accurate Hessian spectra of foundation models have remained out of reach, leading most prior work to rely on small models or strong structural approximations. We show that faithful spectral analysis of the true Hessian is tractable at frontier scale. Using shard-local finite-difference Hessian vector products compatible with Fully Sharded Data Parallelism, we perform stochastic Lanczos quadrature on open-source language models with up to 100B parameters, producing the first large-scale spectral density estimates beyond the sub-10B regime. We characterize the numerical behavior of this pipeline, including finite-difference bias, floating-point noise amplification, and their effect on Krylov stability in fp32 and bf16, and derive practical operating regimes that are validated empirically. We further provide end-to-end runtime and memory scaling laws, showing that full-operator spectral probing incurs only a modest constant-factor overhead over first-order training. Crucially, direct access to the Hessian reveals that widely used block-diagonal curvature approximations can fail catastrophically, exhibiting order-one relative error and poor directional alignment even in mid-scale LLMs. Together, our results demonstrate that foundation-model Hessian spectra are both computable and qualitatively misrepresented by prevailing approximations, opening the door to principled curvature-based analysis at scale.

## 1. Introduction

Second-order information, encapsulated by the Hessian of the training objective is central to understanding and improving modern deep learning systems. Curvature governs optimization dynamics and the efficacy of preconditioning (Martens, 2010; Schraudolph, 2002), reveals the sharpness or flatness of minima associated with generalization (Keskar et al., 2017; Li et al., 2018; Foret et al., 2021), and underpins data attribution tools such as influence functions that require inverse Hessian

vector products (Koh and Liang, 2017). Classically, Hessian vector products (HVPs) provide an efficient, matrix-free primitive for accessing curvature at the cost of a few backpropagations (Pearlmutter, 1994).

At *foundation model scale*, however, computing HVPs becomes a systems problem. State-of-the-art training stacks shard parameters, optimizer states, and activations across devices using data/model parallelism and sharded optimizers (Shoeybi et al., 2019; Rajbhandari et al., 2019; Zhao et al., 2023; Narayanan et al., 2021). Naïvely applying standard HVP routines in these settings typically forces expensive full-parameter gathers, defeating the purpose of sharding and bloating memory and communication. As a result, practical curvature diagnostics, spectral tools, and inverse-Hessian solvers are rarely available during the development and operation of large LMs and vision models, despite their potential to guide training, monitoring, and deployment.

**This paper.** We present a scalable framework for *distributed* HVPs that is compatible with Fully Sharded Data Parallelism (FSDP). Our approach preserves model-parallel parameter partitioning to compute HVPs *without* full gathers, enabling second-order analyses at (sparse and dense) trillion-parameter scale. The resulting primitive unlocks several downstream uses: (i) stochastic Lanczos methods to estimate spectral densities and traces (Hutchinson, 1989; Ubaru et al., 2017b; Chen et al., 2021), (ii) conjugate-gradient (CG) solvers for implicit second-order updates (Hestenes and Stiefel, 1952; Martens, 2010; Nocedal and Wright, 2006), and (iii) scalable influence-function pipelines for data sensitivity (Koh and Liang, 2017). We demonstrate near-linear scaling of our distributed HVPs across language and vision models and show competitive wall-clock overheads relative to first-order training passes.

**Scope.** Our work targets *foundation-model-scale* training and evaluation regimes that already rely on sharding (e.g., FSDP/ZeRO, tensor/pipeline parallelism) (Rajbhandari et al., 2019; Shoeybi et al., 2019; Zhao et al., 2023; Narayanan et al., 2021). We intentionally treat the HVP as a systems primitive, focusing on communication/memory efficiency and on composing the primitive with widely used spectral and inverse-Hessian routines.

## 2. Related Work

**Hessian vector products and second-order optimization.** Fast HVPs via reverse-over-forward automatic differentiation were introduced by Pearlmuter (1994). They enable Krylov methods for Newton/Gauss–Newton steps (e.g., CG) without forming the Hessian (Hestenes and Stiefel, 1952; Nocedal and Wright, 2006). In deep learning, Hessian-free optimization (HF) operationalized these ideas with damping and curvature–vector products (Martens, 2010; Martens and Sutskever, 2011), while Schraudolph (2002) developed efficient curvature–vector products for Fisher/Gauss–Newton approximations.

**Curvature, spectra, and generalization.** A rich line of work uses Hessian spectra to probe loss landscape geometry, training dynamics, and generalization (Sagun et al., 2017; Ghorbani et al., 2019b; Li et al., 2018; Granziol, 2019; Granziol and Baskerville, 2021). Stochastic trace and spectral estimators such as Hutchinson’s method and stochastic Lanczos quadrature (SLQ) make full-spectrum probing feasible using only matvecs (Hutchinson, 1989; Ubaru et al., 2017b; Chen et al., 2021). Practical toolkits such as PyHessian leverage HVPs for moderately sized models (Yao et al., 2019). Recent work reports power-law Hessian spectra but is limited to sub-billion-parameter models (Tang et al., 2025).

**Influence functions and iHVPs.** Influence functions attribute predictions to training examples by computing inverse–Hessian vector products (iHVPs) (Koh and Liang, 2017). Alternative estimators such as TracIn avoid explicit Hessians (Pruthi et al., 2020). Our work enables exact iHVPs at foundation scale.

**Distributed training at scale.** Modern foundation models rely on tensor, pipeline, and sharded data parallelism (Shoeybi et al., 2019; Rajbhandari et al., 2019; Zhao et al., 2023; Narayanan et al., 2021; Fedus et al., 2022; Chowdhery et al., 2022). We target this regime and make HVPs communication-aware.

## 3. Curvature in LLMs: Progress, Motivation, and Contributions

**Why curvature at foundation scale?** Second-order information provides capabilities absent from first-order pipelines: (i) *Monitoring & reliability* via spectral norms and densities to flag instabilities, collapse, or domain shift; (ii) *Optimizer design* through conjugate-gradient implicit updates, damping, or curvature-conditioned schedules (Martens, 2010; No-

cedal and Wright, 2006); (iii) *Data governance* through influence analyses that identify harmful or mislabeled data at scale (Koh and Liang, 2017). Making these tools routine in trillion-parameter regimes promises both efficiency and accountability.

**Recent progress in LLM-scale curvature.** Research has advanced on three complementary fronts.

**Influence functions via curvature approximations.** Bae et al. (2023) scale influence functions using EK-FAC (a K-FAC variant), avoiding explicit inverse–Hessian vector products. While tractable at tens of billions of parameters, this sacrifices exactness and relies on heuristics such as TF-IDF pre-filtering (Anthropic, 2023). **Foundation-scale spectra and tooling.** Granziol et al. (2025) introduce HessFormer, performing Hessian spectral density estimation on 10–70B models via stochastic Lanczos quadrature. The implementation is single-node and limited in FLOP utilisation, restricting scalability. **Hessian structure and geometry.** Tang et al. (2025) report power-law structure in Hessian spectra across CNNs and LLMs, with predictive power for generalization. Complementary work (Di Sipio, 2025) frames LLM optimization through Fisher information geometry.

**Systems challenge.** All of these efforts highlight the importance of curvature but sidestep a key barrier: under FSDP/ZeRO, parameters are sharded, and naïve HVPs force expensive all-gathers. A practical second-order stack must preserve sharding, localize matvecs, and align communication with existing collectives.

### Our contributions.

- **Shard-preserving HVP primitive.** We design Hessian vector products that operate directly on FSDP-sharded parameters, avoiding all-gathers while remaining autograd-compatible.
- **Scalable spectral and inverse–Hessian solvers.** We integrate this primitive with stochastic Lanczos quadrature (Hutchinson, 1989; Ubaru et al., 2017b; Chen et al., 2021) and CG-based inverse–HVP solvers.
- **Empirical scaling.** We demonstrate near-linear strong scaling with node count and modest overhead relative to first-order passes.

**Comparison with recent work.** Table 1 contrasts recent approaches with our shard-preserving HVP framework.

Table 1. Curvature/Hessian methods at LLM scale. ASDL and K-FAC-based systems (PipeFisher, KAISA) target curvature approximations rather than the true Hessian and are not FSDP-native. HessFormer does not scale across GPUs in this regime. In contrast, our primitive preserves FSDP sharding and achieves near-linear scaling.

Work	Method	Scale	Faithfulness
Bae et al. (2023); Anthropic (2023)	IF via EK-FAC (K-FAC)	$10^9\text{--}10^{10}$	Approx.
Granziol et al. (2025)	SLQ + HVP (single node)	$10^{10}\text{--}7 \times 10^{10}$	Exact
Tang et al. (2025)	Empirical Hessian spectra	CNNs, $10^8\text{--}10^9$	Exact (analysis)
Di Sipio (2025)	Fisher/quantum geometry	Conceptual	N/A
<b>Ours</b>	Shard-preserving HVP (FSDP)	$10^{12}+$ (multi-node)	Exact

### 3.1. Shard-local Finite-Difference HvPs under FSDP

We compute dataset-averaged Hessian vector products (HvPs) for FSDP models by a shard-local central finite-difference operator,

$$Hv \approx \frac{\nabla_\theta L(\theta + \varepsilon v) - \nabla_\theta L(\theta - \varepsilon v)}{2\varepsilon}, \quad (1)$$

which discretises the continuous operator  $Hv = \nabla_\theta(D_v L(\theta))$ , with  $D_v L(\theta) = \langle \nabla_\theta L(\theta), v \rangle$ . The perturbations in (1) are applied shard-locally to FSDP parameters, avoiding parameter gathers and preserving data parallelism.

**Theorem 3.1** (Error of gradient finite-difference HvPs). *Let  $L \in C^4(\mathbb{R}^n)$ , let  $\theta \in \mathbb{R}^n$ , and let  $v \in \mathbb{R}^n$  be a unit vector. Consider the gradient finite-difference estimator defined in (1), computed in floating-point arithmetic with machine precision  $\varepsilon_{\text{mach}}$ .*

*Then the approximation error satisfies*

$$\|\tilde{H}v - Hv\| \leq \frac{\varepsilon^2}{6} \|\nabla_\theta(D_v^3 L(\theta))\| + O\left(\frac{\varepsilon_{\text{mach}}}{\varepsilon} \|\nabla_\theta L(\theta)\|\right). \quad (2)$$

Moreover, the error is minimised for

$$\varepsilon^* \asymp \left( \frac{\varepsilon_{\text{mach}} \|\nabla_\theta L(\theta)\|}{\|\nabla_\theta(D_v^3 L(\theta))\|} \right)^{1/3}, \quad (3)$$

at which the minimal achievable error scales as

$$\|\tilde{H}v - Hv\| = O\left(\varepsilon_{\text{mach}}^{2/3} \|\nabla_\theta L(\theta)\|^{2/3} \|\nabla_\theta(D_v^3 L(\theta))\|^{1/3}\right). \quad (4)$$

**Remark 3.2** (Practical step sizes). For float32 arithmetic,  $\varepsilon_{\text{mach}} \approx 1.2 \times 10^{-7}$ , yielding  $\varepsilon^* \sim 10^{-3} 10^{-2}$  and typical HvP errors of order  $10^{-5}$ . For bfloat16,  $\varepsilon_{\text{mach}} \approx 3.9 \times 10^{-3}$ , giving  $\varepsilon^* \sim 10^{-1}$  and HvP errors of order  $10^{-2}$ . These values are consistent with empirical stability observed in large-scale FSDP experiments.

**Algorithm 1** Shard-local finite-difference HVP under FSDP

```

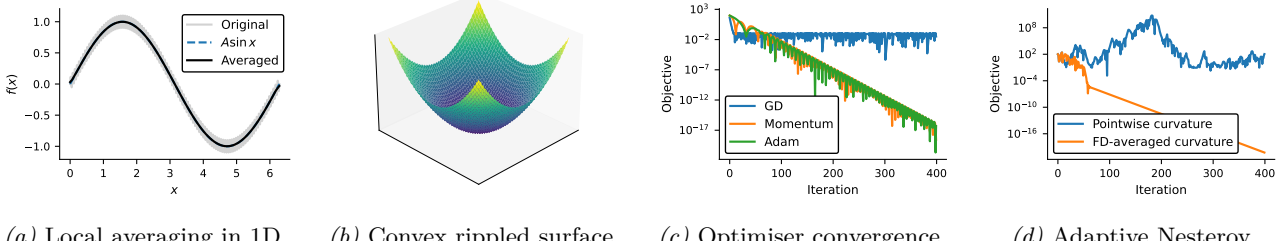
1: Input: parameters  $\theta$ , direction  $v$ , step  $\varepsilon$ , dataloader
2: Output: shard-local Hessian vector product  $Hv$ 
3: Perturb local DTensor shards:  $\theta \leftarrow \theta + \varepsilon v$ 
4: Zero gradients
5: for batch  $b$  in dataloader do
6:   Compute loss  $\ell_b(\theta + \varepsilon v)$ 
7:   Accumulate  $\nabla_\theta \ell_b \cdot w_b$  into param.grad
8: end for
9: Perturb local shards:  $\theta \leftarrow \theta - 2\varepsilon v$  // now at  $\theta - \varepsilon v$ 
10: for batch  $b$  in dataloader do
11:   Compute loss  $\ell_b(\theta - \varepsilon v)$ 
12:   Accumulate  $-\nabla_\theta \ell_b \cdot w_b$  into param.grad
13: end for
14: Restore parameters:  $\theta \leftarrow \theta + \varepsilon v$ 
15: Collect shard-local gradients into FP32 buffers, set param.grad = None
16: Scale by  $2\varepsilon \sum_b w_b$  to obtain local HvP result
17: return shard-local tensors representing  $Hv$ 

```

**FSDP-native HVP primitive.** Algorithm 1 implements a dataset-averaged finite-difference Hessian vector product under FSDP ZeRO-3. Parameter perturbations  $\theta \mapsto \theta \pm \varepsilon v$  are applied *in place* on each rank’s local DTensor shard, avoiding any parameter gathers. Each HVP requires two standard FSDP gradient passes over the same dataloader slice, and three shard-local AXPY updates to restore parameters. The resulting gradients are accumulated locally and scaled by  $(2\varepsilon)^{-1}$ , yielding shard-local pieces of  $Hv$ . Beyond the communication already incurred by FSDP during backpropagation, the only additional collective is at most a scalar all-reduce to normalize  $v$  or form global dot-products in Krylov routines.

### 3.2. Finite Difference as Local Averaging

For a function  $f : \mathbb{R}^n \rightarrow \mathbb{R}$ , the central finite-difference approximation to the directional second derivative



(a) Local averaging in 1D. (b) Convex rippled surface. (c) Optimiser convergence. (d) Adaptive Nesterov

Figure 1. Local averaging suppresses high-frequency curvature without altering large-scale geometry. (a) Finite differences act as a local averaging operator on oscillatory signals. (b) A globally convex surface with high-frequency curvature. (c) Best achievable convergence under grid-searched learning rates for GD, momentum, and Adam for surface (b). (d) Adaptive Nesterov acceleration using pointwise versus finite-difference averaged curvature on surface (b).

along a unit vector  $v$  is

$$H_\varepsilon(x)[v] = \frac{f(x + \varepsilon v) - 2f(x) + f(x - \varepsilon v)}{\varepsilon^2}. \quad (5)$$

This approximation can be written exactly as a weighted average of the true Hessian along the line  $x + tv$ .

**Theorem 3.3.** For  $f \in C^2(\mathbb{R}^n)$ ,

$$H_\varepsilon(x)[v] = \frac{1}{\varepsilon} \int_{-\varepsilon}^{\varepsilon} w_\varepsilon(t) v^\top H(x + tv) v dt, \quad (6)$$

where

$$w_\varepsilon(t) = 1 - \frac{|t|}{\varepsilon}, \quad (7)$$

and  $H(x) = \nabla^2 f(x)$ .

See App. A.1 for proof. The weighting function  $w_\varepsilon$  is nonnegative, symmetric, and supported on  $[-\varepsilon, \varepsilon]$ , with  $\frac{1}{\varepsilon} \int_{-\varepsilon}^{\varepsilon} w_\varepsilon(t) dt = 1$ . It attains its maximum at  $t = 0$  and decays linearly to zero at the boundary, corresponding to a triangular averaging kernel.

As shown in Figure 1a the function

$$f(x) = A \sin x + B \sin(\omega x),$$

or (Figure 1b) its higher dimensional equivalent

$$f(x, y) = \frac{1}{2}(x^2 + y^2) + B \sin(\omega x) \sin(\omega y),$$

where  $w \gg 1$ . Such functions locally have large curvature but are globally smooth. Such a surface exhibits known tendencies in deep learning such as the improved performance of momentum SGD and Adam over SGD (Figure 1c). We find that for this toy problem, setting the per iteration learning rates and Nesterov (Nesterov, 1983) momentum

$$\alpha = \frac{1}{L}, \quad \beta = \frac{\sqrt{L} - \sqrt{m}}{\sqrt{L} + \sqrt{m}}.$$

We find that only pointwise curvature (Figure 1d) converges.

#### 4. (Stochastic) Lanczos (Quadrature)

The Lanczos algorithm approximates eigenvalues of a symmetric matrix via the recurrence

$$\beta_{k+1} q_{k+1} = H q_k - \alpha_k q_k - \beta_k q_{k-1}, \quad \alpha_k = q_k^\top H q_k. \quad (8)$$

After  $m$  steps,  $H$  is approximated by a tridiagonal  $T_m$ , whose Ritz values approximate extremal eigenvalues. In finite precision, loss of orthogonality yields ghost eigenvalues (Paige, 1971). With random probes, Lanczos enables stochastic Lanczos quadrature (SLQ) (Ubaru et al., 2017a), estimating

$$v^\top f(H)v \approx e_1^\top f(T_m)e_1, \quad (9)$$

recovering the spectral density via polynomial moments encoded by the Krylov process. Despite extensive use at moderate scale, SLQ had not been demonstrated at LLM scale due to the cost of repeated HvPs. Our shard-local HvP enables SLQ under FSDP. We quantify how the Lanczos algorithm adapts under finite difference Hessian vector products with the following theorem.

**Theorem 4.1** (Error of Lanczos with finite-difference Hessian vector products). *Let  $H = \nabla^2 f(x) \in \mathbb{R}^{P \times P}$  be symmetric, and let  $\tilde{T}_m$  be the tridiagonal matrix produced by  $m$  steps of the symmetric Lanczos algorithm applied to  $H$ , where Hessian vector products are approximated using the central finite-difference estimator of Theorem 3.1 with step size  $\varepsilon^*$ .*

*Assume the finite-difference errors are unbiased and independent across Lanczos iterations. Then the computed tridiagonal satisfies*

$$\tilde{T}_m = T_m + \Delta T_m,$$

*where the perturbation obeys*

$$\mathbb{E} \|\Delta T_m\|_2 \lesssim \|H\|_2 \sigma_f^{1/2} \|D^4 f\|^{1/2} \sqrt{\frac{m \bar{\eta}}{P}}.$$

Consequently, the Ritz values  $\tilde{\lambda}_i$  satisfy

$$|\tilde{\lambda}_i - \lambda_i| \lesssim \|H\|_2 \sigma_f^{1/2} \|D^4 f\|^{1/2} \sqrt{\frac{m \bar{\eta}}{P}} \quad \text{in expectation.}$$

Moreover, loss of orthogonality among Lanczos vectors induces spurious duplicate (“ghost”) eigenvalues with RMS splitting

$$\Delta\lambda_{\text{ghost}} \sim 2 \|H\|_2 \sigma_f^{1/2} \|D^4 f\|^{1/2} \sqrt{\frac{k \bar{\eta}}{P}},$$

where  $k$  denotes the number of Lanczos iterations after convergence of the associated Ritz vector.

**Remark 4.2.** When the finite-difference step size is chosen optimally as in Theorem 3.1, we reduce to Paiges classic result. The quantity

$$\bar{\eta} \equiv (\mathbb{E}\|q\|_\infty^2)^{-1},$$

where  $q$  denotes a typical Lanczos vector, measures the effective delocalisation of Krylov basis vectors.

## 5. Systems Characterization: Cost, Scaling, and Baselines

Let  $T_{\text{grad}}$  denote the wall-clock time for a single distributed FSDP gradient evaluation: one forward and one backward pass over the dataloader slice, including FSDP parameter all-gathers and gradient reduce-scatter/all-reduce collectives, but no optimizer update. In a standard  $(\alpha, \beta, \gamma)$  model, per rank:

$$T_{\text{grad}} = F_{\text{fwd}} \gamma + F_{\text{bwd}} \gamma + \alpha G_{\text{grad}} + \beta V_{\text{grad}},$$

where  $F_{\text{fwd}}, F_{\text{bwd}}$  are forward/backward FLOPs,  $G_{\text{grad}}$  is the number of collectives invoked by FSDP, and  $V_{\text{grad}}$  is the total communicated payload per rank.

**Cost of one dataset-averaged HVP.** All additional work outside the two FSDP passes consists of linear-time vector operations over  $P_{\text{loc}}$  parameters (AXPYs, copies, scaling) plus at most one scalar all-reduce. Grouping these into  $T_{\text{vec}}$  yields:

$$T_{\text{HVP}} = 2 T_{\text{grad}} + T_{\text{vec}}, \quad T_{\text{vec}} = \mathcal{O}(P_{\text{loc}} \gamma) + \mathcal{O}(T_{\text{scalar}}),$$

where  $T_{\text{scalar}}$  denotes the cost of a scalar all-reduce. Importantly, the HVP has *exactly* the same FSDP communication pattern as two gradient evaluations, and introduces no additional  $\mathcal{O}(P)$ -sized collectives (no full-parameter all-gathers beyond those already implied by FSDP execution).

**Cost of one Lanczos iteration.** Each Lanczos step requires one Hessian vector product, a constant number of global scalar reductions to form recurrence coefficients, and shard-local vector operations. With sliding-window reorthogonalisation of size  $r$ , this incurs at most  $(2+r)$  scalar all-reduces and  $\mathcal{O}((1+r)P_{\text{loc}})$  local AXPY operations. Thus one iteration costs

$$T_{\text{Lanczos iter}}(r) = T_{\text{HVP}} + (2+r) T_{\text{scalar}} + \mathcal{O}\left((1+r) \frac{P}{R} \gamma\right).$$

**End-to-end SLQ/CG complexity (for context).** For stochastic Lanczos quadrature (SLQ) with  $m$  Krylov steps and  $s$  random probe vectors, the total time is

$$T_{\text{SLQ}} \approx s m T_{\text{Lanczos iter}}(r) + T_{\text{post}},$$

where  $T_{\text{post}}$  (tridiagonal eigendecompositions and quadrature) is typically negligible compared to the  $sm$  HVP calls at scale. A CG-based inverse-HVP solver similarly reduces to repeated HVP calls plus scalar reductions and shard-local vector operations, and therefore inherits the same cost structure.

### 5.1. Empirical scaling

Our HVP inherits the asymptotic scaling of a standard FSDP gradient evaluation. In particular, when a model *fits* on a single rank, FSDP ZeRO-3 can be strictly slower than standard data parallelism (DP) because ZeRO-3 trades memory savings for more frequent communication. We formalise this in Appendix B. We display single node scaling results in Table 3 and multi node scaling results in Table 4. As shown in Table 5, for the one available multi-GPU hessian calculation method (Granziol et al., 2025) we see significant (4x) speedups, justifying our contribution at a cost per experiment level.

**Empirical Lanczos overhead** Lanczos adds only shard-local vector operations and scalar reductions on top of two gradient passes. This is a small overall overhead relative to the hessian vector product in typical setups, we confirm this experimentally in Table 2.

## 6. Exp I: Block-diagonal Hypothesis Test

To illustrate analyses enabled by our primitive, we test the common assumption that the Hessian is approximately block diagonal. In optimisation, natural-gradient methods replace the intractable full Fisher Information Matrix with explicit layer-wise block-diagonal approximations, most notably through

**Title Suppressed Due to Excessive Size**

Model	Batch	Steps	Reorth	Subsample	$T_{\text{HVP}}$ (s)	$T_{\text{Lanczos}}$ (s)	Overhead
DeepSeek-R1-Distill-Qwen-7B	1	1	False	1/1000	23.99	24.30	$\approx 1.3\%$
Qwen-1.5B	2	8	True	1/200	71.26	72.53	$\approx 1.8\%$

*Table 2.* Lanczos overhead relative to the HVP primitive.

#GPUs	Avg t	Std	Peak mem	Speedup
1	12.40s	0.05s	67.63GB	1.00×
2	7.93s	0.04s	68.74GB	1.56×
4	4.06s	0.10s	67.22GB	3.05×
8	2.16s	0.03s	66.51GB	5.74×

*Table 3.* Strong scaling of the HVP primitive on one node. Batch size 160 on Qwen 0.6B, sequence length 1024 on wikitext-2.

#Nodes	B	Avg t	Std	Peak mem	Speedup
1	64	9.36s	0.07s	62.70GB	1.00×
2	72	5.20s	0.06s	67.31GB	1.80×

*Table 4.* Multi-node scaling of the HVP primitive.  $B$  denotes batch size and GPU count is  $8 \times$  Nodes. Qwen 32B on wikitext-2 sequence length 1024.

Method	Batch	GPUs	Avg time	Peak mem
HessFormer	32	8	89.57s	71.91GB
FSHP	80	8	22.21s	74.71GB

*Table 5.* Single-node comparison on a 32B Qwen model.

Kronecker-factored approaches such as K-FAC (Amari, 1998; Martens and Grosse, 2015). In pruning, while early second-order methods assumed a diagonal Hessian (LeCun et al., 1990), subsequent work showed that full-Hessian formulations are computationally infeasible beyond small models (Hassibi and Stork, 1993), motivating block-wise and layer-wise approximations in practice. In large-scale post-training quantisation, block-diagonal structure is enforced by design: methods such as GPTQ optimise second-order objectives independently over small parameter blocks using local Hessian approximations, discarding cross-block interactions entirely (Frantar and Alistarh, 2023).

To evaluate the validity of a block-diagonal approximation of the Hessian in transformer layer space, we test whether cross-block curvature terms are negligible in practice. Let  $\theta \in \mathbb{R}^P$  denote the flattened parameter vector, partitioned into contiguous blocks  $\{\theta^{(b)}\}$  corresponding to individual transformer layers. For a randomly sampled probe vector  $v \sim \mathcal{N}(0, I)$  with  $\|v\|_2 = 1$ , we compute the full Hessian vector product

$$h_{\text{full}} = Hv,$$

using a finite-difference estimator over minibatches. For each block  $b$ , we construct a masked probe  $v^{(b)}$  by zeroing all components of  $v$  outside block  $b$ , and

compute the corresponding masked product  $h_{\text{masked}}^{(b)} = Hv^{(b)}$ .

We then restrict both products to the same block and compare  $(Hv)^{(b)}$  with  $(Hv^{(b)})^{(b)}$ , which isolates the contribution of cross-block Hessian terms. Deviations are quantified via the relative error

$$\frac{\|(Hv)^{(b)} - (Hv^{(b)})^{(b)}\|}{\|(Hv)^{(b)}\|},$$

and cosine similarity between the two vectors. If the Hessian were approximately block-diagonal, these quantities would be close to zero and one, respectively.

## 6.1. Model on generic Data

For Qwen-0.6B on WikiText, parameters are split into 28 blocks. For a probe vector  $v$ , we compare  $Hv$  to a block-diagonal proxy  $H_{\text{block}}v$ , the results shown in Table 6. Here we see, that for a general LLM on a general dataset we have an  $O(1)$  magnitude error and some but not overwhelming directional alignment as measured by cosine similarity.

Metric	Mean $\pm$ Std Dev
$\ H_{\text{block}}v - Hv\ $	$0.082 \pm 0.054$
Relative error	$0.941 \pm 0.059$
Cosine similarity	$0.311 \pm 0.120$
Blocks	28

*Table 6.* Block-diagonal approximation error on Qwen-0.6B.

## 6.2. Code generation fine-tuning experiment

We fine-tune a causal language model on a coding dataset using a standard autoregressive objective, with loss applied only to the solution tokens. Each example concatenates a prompt and its corresponding solution, but prompt tokens are masked in the loss so that gradients arise solely from conditional solution generation. Writing  $x = (x_{\text{prompt}}, x_{\text{sol}})$  for the full token sequence, the training objective is

$$\mathcal{L}(\theta) = \sum_{t \in x_{\text{sol}}} \ell(f_{\theta}(x_{\leq t}), x_{t+1}),$$

which concentrates curvature on parameters involved in mapping prompts to solutions rather than prompt encoding alone. Sequences are truncated to a fixed max-

imum length and processed independently. Optimization is performed with AdamW under distributed training using **Accelerate**, with optional gradient checkpointing and mixed-precision arithmetic. The model remains in training mode throughout, ensuring that subsequent Hessian vector products correspond to the true training objective rather than an evaluation-time surrogate, and thus reflect the second-order structure encountered by the optimizer.

Empirically, as shown in Table 7 for Deepseek 1.3Bn coder, in we observe large relative errors and near-zero mean cosine similarity across most blocks, indicating strong cross-layer coupling in the curvature. The only notable exception occurs in the final transformer block, where the cosine similarity is substantially higher, consistent with the reduced downstream mixing and MLP-dominated structure of the last layer.

Metric	Mean $\pm$ Std Dev
$\ H_{\text{block}}v - Hv\ $	$0.00442 \pm 0.00444$
Relative error	$1.214 \pm 0.150$
Cosine similarity	$0.00443 \pm 0.127$
Blocks	24

Table 7. Block-diagonal approximation error (per-block statistics).

## 7. Exp II: Hessian Spectra

Following prior spectral studies (Ghorbani et al., 2019a; Papyan, 2019; Ubaru et al., 2017a), we focus on estimating the spectral density of the Hessian rather than computing individual eigenvalues. To the best of our knowledge, Figure 2 is the first spectral density estimate for causal language models at 100Bn parameter scale. The extremely large negative eigenvalues indi-

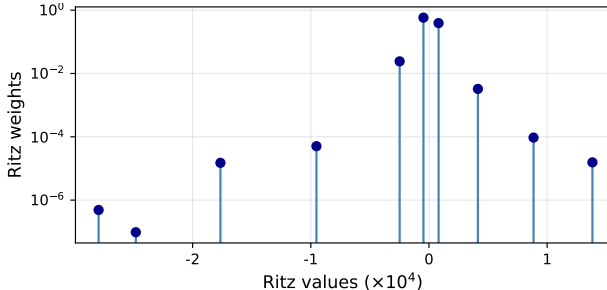


Figure 2. Spectral Density of OpenAI 120Bn parameter open weight model on wikitext-2, sequence length 64,  $\epsilon = 10^{-4}$ .

cate that the data as tokenised has clearly not been memorised (there are directions of steep descent available). This may provide evidence to the problem of hallucination. Recollection of non memorised data will

by definition be lossy. However since we do not know the details of OpenAIs 120Bn model (OpenAI, 2025) training regimen and dataset, the plot is only indicative. We also do not have the resources to run several tests with varying dataset sizes to understand the magnitude of broadening (Granziol, 2019). Due to the model size, only the essential Lanczos vectors were stored (not the entire krylov subspace) and no re-orthogonalisation was performed. Due to the small number of iterations (10) and using Theorems 4.1 & 3.1 we do not see the obvious artefacts of low precision arithmetic distorting our computations, indicating correct analysis within the scale of computation.

### 7.1. Lanczos vectors precision, $\epsilon$ and sub-sampling

Given that our method requires storing the full Krylov subspace in memory<sup>1</sup>, we study the numerical precision required to obtain stable Hessian spectral estimates, as well as the sensitivity of the spectrum to the smoothing parameter  $\epsilon$ .

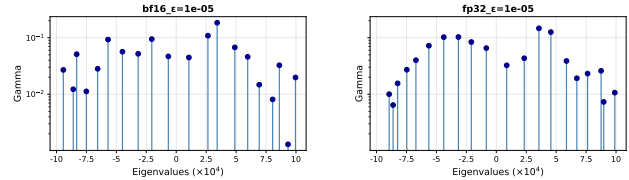


Figure 3. Pairwise structure for  $\epsilon = 10^{-5} \ll \epsilon_{\text{opt}}$ . Matrix spectra resembles that of a random matrix with no clear outlier separation.

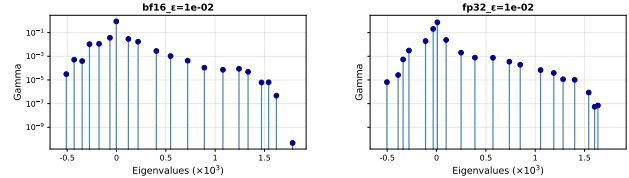


Figure 4. Pairwise structure for  $\epsilon = 10^{-2} \gg \epsilon_{\text{opt}}$ . Matrix spectra resembles that of a random matrix with no clear separation.

We evaluate these effects using the Pythia-160M model trained on the Pile dataset, which we treat as an in-distribution setting for Hessian estimation. Experiments are conducted on a 1% subset of the Pile (1k examples drawn from a 100k-row deduplicated subset). All Lanczos scalar operations -including inner products and entries of the tridiagonal  $T$  matrix -are performed in float32, while only the Lanczos basis vectors are

<sup>1</sup>Future work could offload portions of the subspace to CPU or disk to reduce memory pressure and enable larger-scale runs.

stored in either bfloat16 or float32. We perform a grid search over  $\epsilon$ , apply full re-orthogonalisation at every Lanczos iteration, and retain the entire Krylov subspace.

We use a sequence length of 2048 tokens, padding each batch to the maximum sequence length (capped at 2048) using `pad_token_id` (or `eos_token_id` when unset). Labels are padded with -100, and attention masks assign ones to real tokens and zeros to padding.

Comparing bfloat16 and float32 Lanczos vectors on the same axes, we observe only minimal deviations between the resulting spectra, indicating that bfloat16 storage is sufficient for faithful spectral estimation. Clear Hessian structure, manifested as isolated spectral outliers, emerges for  $10^{-4} \leq \epsilon \leq 10^{-3}$ . Around  $\epsilon \approx 10^{-3}$ , modest differences appear: bfloat16 exhibits mild outlier broadening.

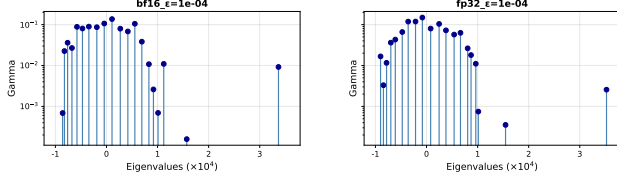


Figure 5. Pairwise structure for  $\epsilon = 10^{-4} \approx \epsilon_{\text{opt.}}$

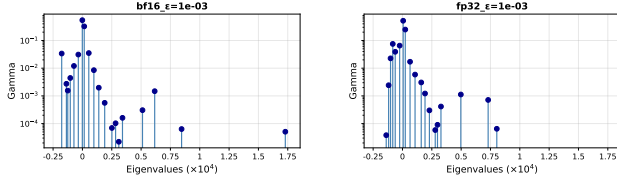


Figure 6. Pairwise structure for  $\epsilon = 10^{-3} \approx \epsilon_{\text{opt.}}$

**Impact of Subsampling:** We find as shown in Figure 7 that increasing the in distribution dataset size by a factor of 30 does not meaningfully alter the spectral distribution. This indicates using random matrix

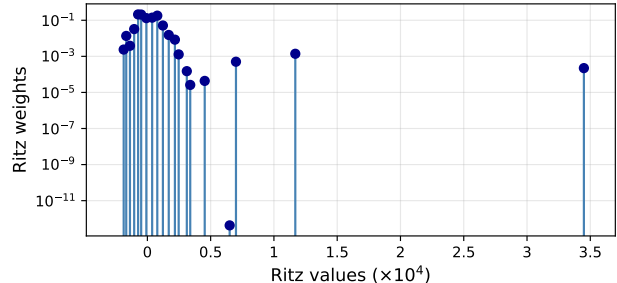


Figure 7. Results for Pythia-160M (bf16) at  $\epsilon = 10^{-4}$  using a 30% subtraining split.

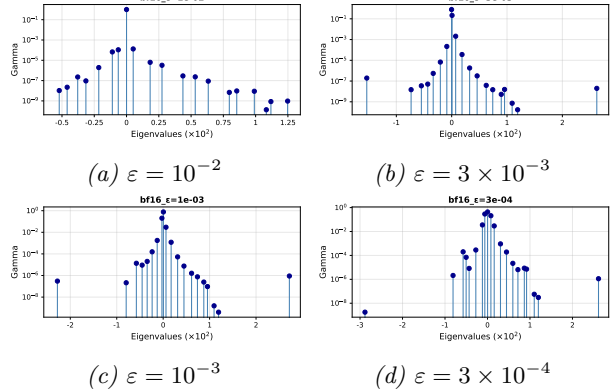


Figure 8. Stem plots of  $\gamma$  versus Hessian eigenvalues for Pythia-1.4B (bf16).

theretic arguments (Graniol, 2019) that the variance per Hessian element  $H_{ij}$  is low. This implies that we expect curvature based methods such as second order or stochastic gradient optimisers to perform well at small batch size and that the curvature based quantisation methods require a small calibration set, both of which are observed in practice.

**Deviations at Scale:** We repeat the same experiment but for a large Pythia 1.4B model and find a relatively consistent spectrum for  $10^{-4} \leq \epsilon \leq 10^{-3}$  as shown in Figure 8. This is an interesting finding not reported in the literature. What this exposes is that larger models trained on the same dataset are more stable in metrics of *global* curvature compared to their smaller counterparts.

## 8. Conclusion

We presented a shard-preserving framework for computing exact Hessian vector products under Fully Sharded Data Parallelism, enabling second-order analysis at the scale of modern foundation models. By avoiding full parameter gathers and aligning curvature computation with existing FSDP communication patterns, our method transforms the Hessian from a theoretical object into a practical systems primitive. Empirically, we demonstrated near-linear scaling across nodes and only modest constant-factor overhead relative to first-order gradient evaluation.

Building on this primitive, we performed stochastic Lanczos quadrature on language models ranging from hundreds of millions to over 100 billion parameters, producing the first Hessian spectral density estimates at true foundation-model scale. We analyzed the numerical behavior of finite-difference Hessian vector products in this regime, characterizing truncation bias, floating-

point noise amplification, and Krylov stability. These analyses yielded concrete operating regimes for the finite-difference step size and Lanczos precision, which were validated empirically across model sizes, precisions, and subsampling levels.

Our results expose qualitative failures of widely used curvature approximations. In particular, we showed that block-diagonal Hessian assumptions—central to natural-gradient methods, influence-function approximations, and post-training quantization—can incur order-one relative error and poor directional alignment even in mid-scale transformer models, with these effects persisting or worsening under fine-tuning. Direct access to the full Hessian reveals strong cross-layer coupling that is systematically discarded by such approximations.

Beyond methodology, our findings suggest that global curvature statistics stabilize with scale: larger models trained on the same data exhibit more robust Hessian spectral structure across a wide range of finite-difference step sizes and subsampling ratios. This observation, which has not been previously reported, points to a form of emergent regularity in large-scale optimization landscapes and has implications for curvature-aware optimization, monitoring, and compression.

Taken together, our work establishes that faithful Hessian analysis is not only feasible but informative at foundation-model scale. By making exact curvature accessible under realistic distributed training regimes, we open the door to principled second-order optimization, reliable influence analysis, and quantitatively grounded model compression for the next generation of large-scale models.

From a practical standpoint, our results indicate that storing Lanczos basis vectors in bfloat16—while retaining float32 arithmetic for scalar operations—is sufficient to recover stable Hessian spectra in large language models, substantially reducing memory overhead without compromising spectral fidelity.

## Broader Impact

This work advances the practical accessibility of second-order information for large-scale machine learning systems by making faithful Hessian analysis tractable under realistic distributed training regimes. By enabling curvature-based diagnostics, optimization, and analysis at foundation-model scale, the methods introduced here may contribute to improved training stability, more efficient optimization, and better-informed model compression and deployment strategies. In particular, reliable access to Hessian spectra can support early detection of training pathologies, principled tuning of optimization hyperparameters, and more transparent assessment of model sensitivity to data and parameter perturbations.

At the same time, the techniques described in this paper are primarily infrastructural and analytical in nature. They do not directly introduce new model capabilities, nor do they alter the functional behavior of trained models. As such, we do not anticipate direct societal harms arising uniquely from the use of these methods. However, like many advances in large-scale machine learning infrastructure, improved optimization and analysis tools may indirectly lower the cost of training or refining high-capacity models, potentially accelerating the deployment of powerful systems. Responsible use therefore requires that practitioners continue to apply appropriate safeguards, evaluation protocols, and governance mechanisms when developing and deploying large models.

We also note that our findings highlight limitations of commonly used curvature approximations, such as block-diagonal Hessian assumptions, which are often employed in downstream tasks including model compression and influence analysis. While exposing these limitations can lead to more reliable methods, misuse or misinterpretation of approximate curvature information could result in misleading conclusions if applied without validation. We encourage practitioners to treat curvature-based tools as diagnostic aids rather than definitive measures, particularly when applied outside the regimes studied here.

Overall, we view this work as enabling more principled and transparent analysis of large-scale learning dynamics. By improving access to exact curvature information, it has the potential to support safer, more reliable, and better-understood foundation models when combined with responsible engineering and deployment practices.

## References

Shun-ichi Amari. Natural gradient works efficiently in learning. *Neural Computation*, 1998.

Anthropic. Studying large language model generalization with influence functions, 2023. URL <https://www.anthropic.com/research/studying-large-language-model-generalization-with-influence-functions>. Research blog.

Juhan Bae, Cem Anil, Nelson Elhage, Alex Tamkin, Amirhossein Tajdini, Benoit Steiner, Dustin Li, Esin Durmus, Ethan Perez, Evan Hubinger, Kamilé Lukošiūtė, Karina Nguyen, Nicholas Joseph, Sam McCandlish, Jared Kaplan, Samuel R. Bowman, and Roger Grosse. Studying large language model generalization with influence functions. *arXiv:2308.03296*, 2023. URL <https://arxiv.org/abs/2308.03296>.

Tyler Chen, Thomas Trogdon, and Shashanka Ubaru. Analysis of stochastic lanczos quadrature for spectrum approximation. In *ICML*, 2021.

Aakanksha Chowdhery et al. Palm: Scaling language modeling with pathways. *arXiv:2204.02311*, 2022.

Riccardo Di Sipio. Rethinking llm training through information geometry and quantum metrics. *arXiv:2506.15830*, 2025. URL <https://arxiv.org/abs/2506.15830>.

William Fedus, Barret Zoph, and Noam Shazeer. Switch transformers: Scaling to trillion parameter models with simple and efficient sparsity. *JMLR*, 23(120):1–39, 2022.

Pierre Foret, Ariel Kleiner, Hossein Mobahi, and Behnam Neyshabur. Sharpness-aware minimization for efficiently improving generalization. In *ICLR*, 2021.

Elias Frantar and Dan Alistarh. Gptq: Accurate post-training quantization for generative pre-trained transformers. In *International Conference on Learning Representations*, 2023.

Amir Ghorbani, Rishab Krishnan, and Ying Xiao. An investigation into neural network hessians. In *International Conference on Machine Learning*, 2019a.

Behrooz Ghorbani, Shankar Krishnan, and Ying Xiao. An investigation into neural net optimization via hessian eigenvalue density. In *ICML*, 2019b.

Diego Granziol. Learning rates as a function of batch size: A random matrix theory approach to neural network training. In *Advances in Neural Information Processing Systems*, 2019.

Diego Granziol and Nicholas Baskerville. Spectrum of deep learning: Universality, random matrix theory and neural tangents. *arXiv preprint arXiv:2102.06740*, 2021.

Diego Granziol et al. Hessformer: Hessians at foundation scale. *arXiv:2505.11564*, 2025. URL <https://arxiv.org/abs/2505.11564>.

Babak Hassibi and David Stork. Second order derivatives for network pruning: Optimal brain surgeon. *Advances in Neural Information Processing Systems*, 1993.

Magnus R. Hestenes and Eduard Stiefel. Methods of conjugate gradients for solving linear systems. *Journal of Research of the National Bureau of Standards*, 49(6):409–436, 1952.

Michael F. Hutchinson. A stochastic estimator of the trace of the influence matrix for laplacian smoothing splines. *Communications in Statistics: Simulation and Computation*, 18(3):1059–1076, 1989.

Nitish Shirish Keskar, Dheevatsa Mudigere, Jorge Nocedal, Mikhail Smelyanskiy, and Ping Tak Peter Tang. On large-batch training for deep learning: Generalization gap and sharp minima. In *ICLR*, 2017.

Pang Wei Koh and Percy Liang. Understanding black-box predictions via influence functions. In *ICML*, 2017.

Yann LeCun, John Denker, and Sara Solla. Optimal brain damage. *Advances in Neural Information Processing Systems*, 1990.

Hao Li, Zheng Xu, Gavin Taylor, Christoph Studer, and Tom Goldstein. Visualizing the loss landscape of neural nets. In *NeurIPS*, 2018.

James Martens. Deep learning via hessian-free optimization. In *ICML*, pages 735–742, 2010.

James Martens and Roger Grosse. Optimizing neural networks with kronecker-factored approximate curvature. In *International Conference on Machine Learning*, 2015.

James Martens and Ilya Sutskever. Learning recurrent neural networks with hessian-free optimization. In *ICML*, pages 1033–1040, 2011.

Deepak Narayanan, Mohammad Shoeybi, Jared Casper, Patrick LeGresley, Mostofa Patwary, Vijay Anand Korthikanti, Dmitri Vainbrand, Prethvi Kashinkunti, Julie Bernauer, Bryan Catanzaro, Amar Phanishayee, and Matei Zaharia. Efficient large-scale language

model training on gpu clusters using megatron-lm. *arXiv:2104.04473*, 2021.

Yurii Nesterov. A method for solving the convex programming problem with convergence rate  $\mathcal{O}(1/k^2)$ . *Doklady Akademii Nauk SSSR*, 269(3):543–547, 1983.

Jorge Nocedal and Stephen J. Wright. *Numerical Optimization*. Springer, 2 edition, 2006.

OpenAI. gpt-oss-120b & gpt-oss-20b model card, 2025. URL <https://arxiv.org/abs/2508.10925>.

Christopher C. Paige. *The computation of eigenvalues and eigenvectors of very large sparse matrices*. PhD thesis, University of London, 1971.

Vardan Papyan. Measurements of neural network Hessians reveal the role of overparameterization. In *Advances in Neural Information Processing Systems*, 2019.

Barak A. Pearlmutter. Fast exact multiplication by the hessian. *Neural Computation*, 6(1):147–160, 1994. doi: 10.1162/neco.1994.6.1.147.

Garima Pruthi, Frederick Liu, Satyen Kale, and Mukund Sundararajan. Estimating training data influence by tracing gradient descent. In *NeurIPS*, 2020.

Samyam Rajbhandari, Jeff Rasley, Olatunji Ruwase, and Yuxiong He. Zero: Memory optimizations toward training trillion parameter models. *arXiv:1910.02054*, 2019.

Levent Sagun, Utku Evci, V. Ugur Guney, Yann Dauphin, and Léon Bottou. Empirical analysis of the hessian of over-parametrized neural networks. *arXiv:1706.04454*, 2017.

Nicol N. Schraudolph. Fast curvature matrix-vector products for second-order gradient descent. *Neural Computation*, 14(7):1723–1738, 2002.

Mohammad Shoeybi, Mostofa Patwary, Raul Puri, Patrick LeGresley, Jared Casper, and Bryan Catanzaro. Megatron-lm: Training multi-billion parameter language models using model parallelism. *arXiv:1909.08053*, 2019.

Qian-Yuan Tang, Yufei Gu, Yunfeng Cai, Mingming Sun, Ping Li, Zhou Xun, and Zeke Xie. Investigating the overlooked hessian structure: From cnns to llms. In *International Conference on Machine Learning (ICML)*, Poster, 2025. URL <https://icml.cc/virtual/2025/poster/44080>. Poster ID #44080.

Shashanka Ubaru, Jie Chen, and Yousef Saad. Fast estimation of traces of functions of large matrices via stochastic lanczos quadrature. *SIAM Journal on Matrix Analysis and Applications*, 38(4):1075–1099, 2017a.

Shashanka Ubaru, Jingdong Chen, and Yousef Saad. Fast estimation of  $\text{tr}(f(a))$  via stochastic lanczos quadrature. *SIAM Journal on Matrix Analysis and Applications*, 38(4):1075–1099, 2017b.

Zhewei Yao, Amir Gholami, Kurt Keutzer, and Michael W. Mahoney. Pyhessian: Neural networks through the lens of the hessian. *arXiv:1912.07145*, 2019.

Yanli Zhao, Andrew Gu, Rohan Varma, Liang Luo, Chien-Chin Huang, Min Xu, Less Wright, Hamid Shojanazeri, Myle Ott, Sam Shleifer, Alban Desmaison, Can Balioglu, Pritam Damania, Bernard Nguyen, Geeta Chauhan, Yuchen Hao, Ajit Mathews, and Shen Li. Pytorch fsdp: Experiences on scaling fully sharded data parallel. *arXiv:2304.11277*, 2023.

## A. Understanding Finite Difference Hessian Approximations

*Proof.* Expanding  $\nabla_\theta L(\theta \pm \varepsilon v)$  in a Taylor series around  $\theta$  yields

$$\nabla_\theta L(\theta \pm \varepsilon v) = \nabla_\theta L(\theta) \pm \varepsilon H v + \frac{\varepsilon^2}{2} \nabla_\theta (D_v^2 L(\theta)) \pm \frac{\varepsilon^3}{6} \nabla_\theta (D_v^3 L(\theta)) + O(\varepsilon^4).$$

Subtracting the two expansions and dividing by  $2\varepsilon$  gives

$$\tilde{H}v = H v + \frac{\varepsilon^2}{6} \nabla_\theta (D_v^3 L(\theta)) + O(\varepsilon^4),$$

which yields the truncation error term. Each gradient evaluation is subject to relative floating-point error of order  $\varepsilon_{\text{mach}}$ , which is amplified by subtracting nearly equal vectors, resulting in a dominant roundoff contribution of magnitude  $O(\varepsilon_{\text{mach}} \|\nabla_\theta L(\theta)\|/\varepsilon)$ . Balancing the leading truncation and roundoff terms yields the stated optimal step size and error scaling.  $\square$

*Proof.* We decompose the approximation error into a deterministic truncation (bias) term and a stochastic finite-precision noise term.

**Truncation (Bias) Error.** Since  $f \in C^4(\mathbb{R}^n)$ , a Taylor expansion of the directional curvature along the line  $x + tv$  yields

$$\begin{aligned} v^\top H(x + tv)v &= v^\top H(x)v + t D^3 f(x)[v, v, v] \\ &\quad + \frac{t^2}{2} D^4 f(x)[v, v, v, v] + O(t^3). \end{aligned} \quad (10)$$

Substituting this expansion into the averaging representation of  $H_\varepsilon(x)[v]$  and using the symmetry of the weighting kernel  $w_\varepsilon$  eliminates the odd-order term, since

$$\int_{-\varepsilon}^{\varepsilon} t w_\varepsilon(t) dt = 0. \quad (11)$$

The leading bias term is therefore

$$\frac{1}{\varepsilon} \int_{-\varepsilon}^{\varepsilon} \frac{t^2}{2} D^4 f(x)[v^{\otimes 4}] w_\varepsilon(t) dt. \quad (12)$$

A direct computation gives

$$\frac{1}{\varepsilon} \int_{-\varepsilon}^{\varepsilon} t^2 w_\varepsilon(t) dt = \frac{\varepsilon^2}{6}, \quad (13)$$

so that

$$H_\varepsilon(x)[v] = v^\top H(x)v + \frac{\varepsilon^2}{12} D^4 f(x)[v^{\otimes 4}] + O(\varepsilon^4). \quad (14)$$

Consequently, the deterministic truncation error satisfies

$$|H_\varepsilon(x)[v] - v^\top H(x)v| \leq C_1 \varepsilon^2 \|D^4 f\|. \quad (15)$$

**Finite-Precision and Noise Error.** With noisy function evaluations,

$$\tilde{H}_\varepsilon(x)[v] = H_\varepsilon(x)[v] + \frac{\eta(x + \varepsilon v) - 2\eta(x) + \eta(x - \varepsilon v)}{\varepsilon^2}. \quad (16)$$

Since the noise terms are independent with variance  $\sigma_f^2$ , the variance of the noise contribution is

$$\text{Var}(\tilde{H}_\varepsilon) = \frac{6\sigma_f^2}{\varepsilon^4}, \quad (17)$$

implying a root-mean-square noise error of order

$$O\left(\frac{\sigma_f}{\varepsilon^2}\right). \quad (18)$$

**Combination and Optimisation.** Combining truncation and noise contributions yields

$$\text{Error}(\varepsilon) = O\left(\varepsilon^2 \|D^4 f\|\right) + O\left(\frac{\sigma_f}{\varepsilon^2}\right). \quad (19)$$

Balancing the two terms gives  $\varepsilon_{\text{opt}} \asymp (\sigma_f / \|D^4 f\|)^{1/4}$ , and substituting this value yields the stated minimal error scaling.  $\square$

### A.1. Finite Difference as Local Averaging

**Theorem A.1.** For  $f \in C^2(\mathbb{R}^n)$ ,

$$H_\varepsilon(x)[v] = \frac{1}{\varepsilon} \int_{-\varepsilon}^{\varepsilon} w_\varepsilon(t) v^\top H(x + tv) v dt, \quad (20)$$

where

$$w_\varepsilon(t) = 1 - \frac{|t|}{\varepsilon}, \quad (21)$$

and  $H(x) = \nabla^2 f(x)$ .

*Proof.* From the integral form of Taylor's theorem,

$$f(x + \varepsilon v) = f(x) + \varepsilon \nabla f(x)^\top v + I_+(x), \quad (22)$$

with

$$I_+(x) = \int_0^{\varepsilon} (\varepsilon - t) [v^\top H(x + tv) v] dt. \quad (23)$$

Similarly,

$$f(x - \varepsilon v) = f(x) - \varepsilon \nabla f(x)^\top v + I_-(x), \quad (24)$$

where

$$I_-(x) = \int_0^{\varepsilon} (\varepsilon - t) [v^\top H(x - tv) v] dt. \quad (25)$$

Adding the two expansions yields

$$f(x + \varepsilon v) + f(x - \varepsilon v) - 2f(x) = I_+(x) + I_-(x). \quad (26)$$

Combining the integrals gives

$$I_+(x) + I_-(x) = \int_0^{\varepsilon} (\varepsilon - t) \Xi(t) dt, \quad (27)$$

with

$$\Xi(t) = v^\top H(x + tv) v + v^\top H(x - tv) v. \quad (28)$$

By symmetry,

$$\int_0^{\varepsilon} (\varepsilon - t) \Xi(t) dt = \int_{-\varepsilon}^{\varepsilon} (\varepsilon - |t|) v^\top H(x + tv) v dt. \quad (29)$$

Dividing by  $\varepsilon^2$  gives  $\frac{f(x + \varepsilon v) - 2f(x) + f(x - \varepsilon v)}{\varepsilon^2} =$

$$\frac{1}{\varepsilon} \int_{-\varepsilon}^{\varepsilon} \left(1 - \frac{|t|}{\varepsilon}\right) v^\top H(x + tv) v dt, \quad (30)$$

which proves the claim.  $\square$

## B. FSDP vs DP for small models

To formalise the less than linear scaling for FSDP vs DP in the regime where both fit on memory, let  $C$  be the single-GPU compute time for a step,  $K$  the number of data-parallel ranks,  $P$  the total parameter size (bytes), and  $(\alpha, \beta)$  the latency/bandwidth costs of a ring all-reduce.

Under DP, a step consists of compute plus (approximately) one gradient all-reduce:

$$T_{\text{DP}} = \frac{C}{K} + \alpha(K-1) + 2\beta P. \quad (31)$$

Under FSDP ZeRO-3, parameters are all-gathered and gradients are reduce-scattered at *block granularity*. If the transformer is wrapped into  $L$  FSDP units, then both forward and backward invoke per-block collectives, yielding a higher communication frequency:

$$T_{\text{FSDP}} = \frac{C}{K} + 4\alpha(K-1)L + 8\beta P, \quad (32)$$

where constants reflect that (i) all-gathers/reduce-scatters occur repeatedly across blocks and (ii) parameters/gradients are communicated multiple times across the two passes.<sup>2</sup>

Subtracting (31) from (32) gives

$$T_{\text{FSDP}} - T_{\text{DP}} = 4\alpha(K-1)(L-1) + 6\beta P > 0, \quad (33)$$

so ZeRO-3 is provably slower than DP whenever the model fits in memory and both regimes are feasible.

For deep transformers where communication is a substantial fraction of step time (e.g.,  $L \approx 32\text{-}48$  on  $8\times\text{A100}$ ), it is realistic to have  $T_{\text{comp}} \approx 80\text{ms}$ ,  $T_{\text{DP,comm}} \approx 20\text{ms}$ , and  $T_{\text{FSDP,comm}} \approx 55\text{ms}$ , yielding:

$$T_{\text{DP}} \approx 100\text{ms}, \quad T_{\text{FSDP}} \approx 135\text{ms}, \quad \frac{T_{\text{FSDP}} - T_{\text{DP}}}{T_{\text{DP}}} \approx 0.35. \quad (34)$$

This order-of-magnitude slowdown matches what one should expect when choosing ZeRO-3 in a regime where DP is also possible. We emphasise that our contribution is not to optimise FSDP itself, but to provide an HVP/Lanczos wrapper whose cost profile *tracks* the underlying FSDP backend.

## C. Appendix C: Detailed Cost Breakdown for Distributed Lanczos

This appendix provides a detailed accounting of the computational and communication costs incurred by

<sup>2</sup>The exact constants depend on overlap and implementation details; the key point is the *linear dependence on  $L$*  in the latency term and the larger effective bandwidth term relative to DP.

one distributed Lanczos iteration under FSDP ZeRO-3, complementing the high-level cost expressions given in the main text.

**Cost of one dataset-averaged HVP.** All additional work outside the two FSDP gradient passes consists of linear-time shard-local vector operations over  $P_{\text{loc}} = P/R$  parameters (AXPY updates, copies, and scaling), plus at most one scalar all-reduce. Grouping these operations into  $T_{\text{vec}}$ , the cost of one dataset-averaged Hessian vector product is

$$T_{\text{HVP}} = 2T_{\text{grad}} + T_{\text{vec}}, \quad T_{\text{vec}} = \mathcal{O}(P_{\text{loc}} \gamma) + \mathcal{O}(T_{\text{scalar}}), \quad (35)$$

where  $\gamma$  denotes the cost per shard-local vector operation and  $T_{\text{scalar}}$  the latency of a scalar all-reduce. Importantly, the HVP introduces no additional  $O(P)$ -sized collectives beyond those already implied by FSDP execution.

**Lanczos iteration mechanics.** At iteration  $t$ , each rank stores shard-local pieces of the current and previous Lanczos vectors  $v_t$  and  $v_{t-1}$ . Given the Hessian vector product  $w \leftarrow Hv_t$ , global recurrence coefficients are formed via scalar reductions,

$$\alpha_t = \langle w, v_t \rangle, \quad \beta_t = \|w\|_2, \quad (36)$$

followed by the standard three-term recurrence

$$w \leftarrow w - \alpha_t v_t - \beta_t v_{t-1}, \quad v_{t+1} \leftarrow \frac{w}{\|w\|_2}. \quad (37)$$

All vector updates are performed shard-locally.

**Reorthogonalisation.** When reorthogonalisation is enabled with a sliding window of size  $r$ , the vector  $w$  is additionally orthogonalised against up to  $r$  previously stored Lanczos vectors. Each reorthogonalisation step requires one global dot product (scalar all-reduce) and one shard-local AXPY update.

**Per-iteration cost.** Let  $c_0, c_1 > 0$  be constants capturing the number of shard-local vector operations required per iteration, excluding the Hessian vector product. Then the cost of one Lanczos iteration with window size  $r$  is

$$T_{\text{Lanczos iter}}(r) = T_{\text{HVP}} + (2+r)T_{\text{scalar}} + (c_0 + c_1 r)P_{\text{loc}} \gamma. \quad (38)$$

Substituting  $P_{\text{loc}} = P/R$  yields the expanded expression

$$T_{\text{Lanczos iter}}(r) = 2T_{\text{grad}} + T_{\text{vec}} + (2+r)T_{\text{scalar}} + (c_0 + c_1 r)\frac{P}{R} \gamma. \quad (39)$$

**End-to-end complexity.** For stochastic Lanczos quadrature (SLQ) with  $m$  Krylov steps and  $s$  probe vectors, the total runtime is approximately

$$T_{\text{SLQ}} \approx s m T_{\text{Lanczos iter}}(r) + T_{\text{post}}, \quad (40)$$

where  $T_{\text{post}}$  accounts for tridiagonal eigendecompositions and quadrature evaluation and is typically negligible relative to the  $sm$  HVP calls at scale. Conjugate-gradient-based inverse-HVP solvers admit an analogous cost structure, differing only in constant factors.